

Binding of Dual-Function Hybridized Metal–Organic Capsules to Enzymes for Cascade Catalysis

Junkai Cai, Liang Zhao,* Yanan Li, Cheng He, Chong Wang, and Chunying Duan*



Cite This: *JACS Au* 2022, 2, 1736–1746



Read Online

ACCESS |



Metrics & More



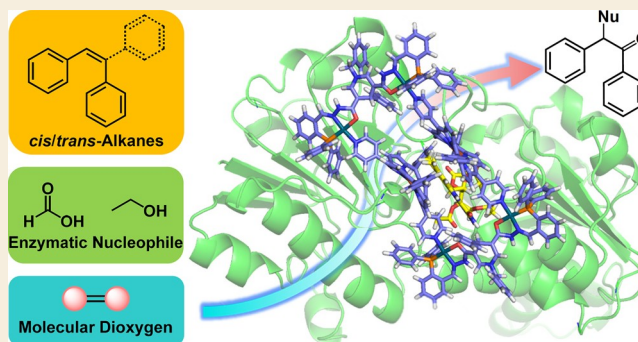
Article Recommendations



Supporting Information

ABSTRACT: The combination of chemo- and biocatalysis for multistep syntheses provides attractive advantages in terms of evolvability, promiscuity, and sustainability striving for desirable catalytic performance. Through the encapsulation of flavin analogues by both NADH and heme mimics codecorated heteroleptic metal–organic capsules, herein, we report a progressive host–guest strategy to imitate cytochrome P450s catalysis for cascade oxidative coupling catalysis. Besides the construction of stable dual-function metal–organic capsules and the modification of cofactor-decorated capsules at the domain of enzymes, this supramolecular strategy involves multistage directional electron flow, affording reactive ferric peroxide species for inducing oxygenation. Under light irradiation, the metal–organic capsule selectively converts stilbene to oxidative coupling products (including 2-oxo-1,2-diphenylethyl formate, 2-alkoxy-1,2-diphenylethanone) in tandem with enzymatic reactions respectively, at the domain of natural enzymes. The ingenious combination of capsules and enzymes with the in situ-regenerated capsule-loaded NADH cofactor promises non-native coupling reactions by forming regional cooperation and division. This abiotic–biotic conjugated host–guest strategy is conducive to the de novo creation of multifunctional components approaching active enzymatic sites for reinforced matter and energy transporting, demonstrating a key role of multicomponent supramolecular catalysts for one-pot integrated catalytic conversions.

KEYWORDS: metal–organic capsule, artificial cytochrome P450s, supramolecular catalysis, C–H bond functionalization, abiotic–biotic system, orthogonal cascades



INTRODUCTION

Supramolecular approaches to combining established natural enzymes with artificial catalysts have emerged as a vital form to achieve efficient and selective catalytic conversions in a bio-orthogonal way.^{1–6} The fabrication of disparate abiological functional groups within the active domain of enzymes in bioinorganic hybrid systems is becoming a highly promising route toward unusual catalytic results immersed in one-pot intricate catalytic networks.^{7,8} The main obstacles to obtain such multifunctional integrated catalytic systems extend beyond the repetition of enzymatic processes and the conquest of inherent communication barrier between abiotic and biotic catalysis.^{9,10} It is more necessary to tackle the synchronous creation of divergent active moieties into enzyme protein scaffolds with considerable compatibility and ensure the fine synergy of multiple functional components, which remains largely elusive. It should be noted that the overall catalytic efficiency of these hybrid biomanufacturing manifolds strongly relies on the shuttling of energy-carrying cofactors, for example, NAD⁺/NADH (nicotinamide adenine dinucleotide pair) between the active centers of enzymes and abiotic catalysis.^{11,12} We envisioned that the incorporation of cofactor

NADH and its mimics^{13,14} into the surface of a catalyst-functionalized heteroleptic assembly would be an ideal toolkit to combine multiple individual active sites into catalytic pockets of enzymes,^{15,16} enabling biological cascades by merging abiotic catalysis with cofactor-dependent enzymatic reactions in one working module.^{17,18} Complementary to biological engineering, such approaches struggle to provide general solutions across gene expression limitation¹⁹ and allow orthogonal cascades by compartmentalization,²⁰ making organic syntheses economically and ecologically worth undertaking.

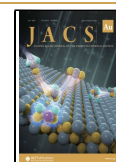
In recent decades, the development of preparative and functionally diverse substrate C–H oxidations has captured particular attention to incorporate oxidized functionality selectively into organic frameworks.^{21,22} Heme-dependent

Received: May 25, 2022

Revised: June 23, 2022

Accepted: June 24, 2022

Published: July 6, 2022



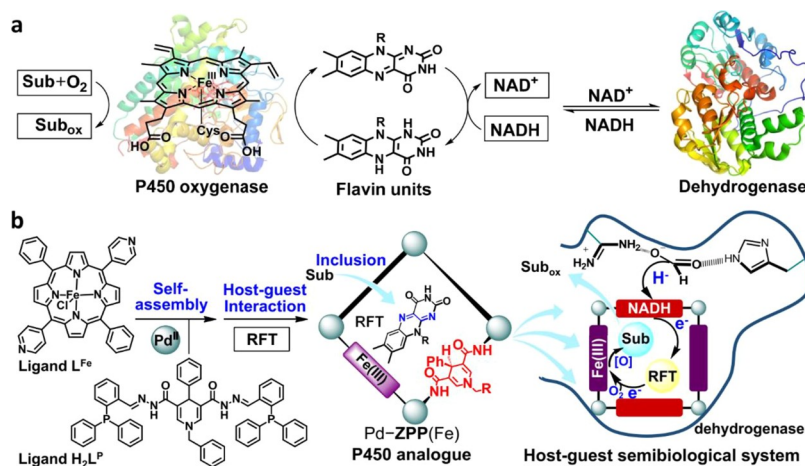


Figure 1. Comparison of natural and artificial tandem catalysis. (a) Multi-enzyme cascades comprising flavin-mediated cytochrome P450 oxygenase and dehydrogenase connected by the diffusion of nicotinamide cofactor couple (NADH/NAD⁺). (b) Construction of the heteroleptic metal–organic capsule Pd–ZPP(Fe) with both NADH and heme model comodified ligands through self-assembly for mimicking cytochrome P450s via encapsulating flavin analogue RFT, combining artificial and natural catalysis within enzymatic pockets by virtue of cofactor channels for a host–guest semibiological system applying to in situ biomimetic oxidation.

cytochrome P450s in nature potentially catalyze a myriad of chemical reactions via the collaboration of multiple functional units using environmentally benign molecular dioxygen as the green oxygen source, capable of operating isolated inactive C–H bond oxidation with predictable selectivity and holding a promise for streamlining syntheses. The catalytic mechanism involves the delivery of electrons originating from NADH through the reduced form of the flavin cofactor to the heme center, in which the reduction activation of O₂ affords a ferric peroxide species for performing C–H functionalization transformations.^{23–25} Accordingly, we hypothesized that both NADH and heme models comodified metal–organic capsules should be ideally applicable for replicating cytochrome P450s by encapsulating a flavin cofactor.^{26–28} This unique approach ensures the integration of all functional components of cytochrome P450s within one assembly, shortening the distance between NADH, flavin, and porphyrin modules, which is applied to strengthen the electron transfer chain and immobilize the electron flow originally occurred in cytochrome P450s.^{29–31} Multiple exogenous catalytic sites can be created nearby natural active sites when artificial hosts bind to the enzymatic pockets, offering a potential way for distinctive catalytic results.⁸ In this case, NADH mimics modified on the host would work as proton- and electron-transport channels for in situ-communicating artificial and natural catalysis inside and outside capsules.^{17,18}

Herein, a coordination-site engineering approach using 3:1 complementary denticity in symmetry interaction is harnessed to build a new heteroleptic metal–organic rectangle with both NADH and heme analogues installing into the backbone of the supramolecular assembly,^{32,33} which engulfs a flavin model, riboflavin tetraacetate (RFT),³⁴ to work as a sophisticated cytochrome P450 oxygenase analogue for oxidative cascade catalysis in tandem with dehydrogenases (Figure 1). The coexistence of NADH, flavin, and heme models within one microenvironment enhances the electron transfer from the NADH module via RFT to the Fe(III)-porphyrin site under irradiation,³⁵ affording oxygen-mediated Fe(IV)-oxo species for catalytic oxidation inside the artificial host. The in situ-formed intermediate within capsules can even react with enzymatic nucleophilic substrates to obtain coupling products.

Thereinto, the cofactors modified on the surface of capsules serving as electron and proton relays in direct contact two catalytic cycles when capsules bind to dehydrogenases, allowing emergence of orthogonal cascades for non-native catalysis in a closed abiotic–biotic catalytic cycle and shifting the paradigm in enzyme modification.

RESULTS AND DISCUSSION

Preparation and Structural Characterization of Metal–Organic Hosts

With the principle of a symmetry interaction strategy using 3:1 complementary denticity as well as the bonding direction approach taken in mind,³⁶ a new heteroleptic metal–organic capsule was able to be developed through co-assembly of three individual components, including NADH active mimic modified ligands (ligand H₂L^P) with NOP tridentate coordinating sites,³⁷ monodentate heme analogue Fe(III)-porphyrin ligands (ligand L^{Fe}), and kinetically inert square planar Pd(II) ions. The ligand H₂L^P was easily obtained by the Schiff base reaction of 2-(diphenylphosphino)benzaldehyde and 1-benzyl-4-phenyl-1,4-dihydropyridine-3,5-dicarbohydrazide in ethanol solution (Figure S1), while the other ligand L^{Fe} was prepared by the condensation reaction of *meso*-phenyl-dipyrromethane and 4-pyridinecarboxaldehyde followed by iron metallization (Figure S2). Through proportioning the ligand H₂L^P, ligand L^{Fe}, and palladium salt at a ratio of 1:1:2 in *N,N*-dimethylformamide (DMF) solution, the dark red paramagnetic target compound (denoted as Pd–ZPP(Fe)) was successfully obtained at room temperature by means of both one-pot and stepwise assembly strategies (Figure S3). Likewise, a nonparamagnetic compound (denoted as Pd–ZPP(H)) possessing the same structural configuration as Pd–ZPP(Fe) was also fabricated by substituting Fe(III)-porphyrin ligands (ligand L^{Fe}) to H-porphyrin ligands (ligand L^H), serving as an ideal reference compound for Pd–ZPP(Fe) to grasp structure information and investigate host–guest and catalytic behavior of capsules in the collaborative catalysis with natural enzymes.

The paramagnetic property of Fe(III)-porphyrin units on Pd–ZPP(Fe) was manifested by the broadening signals

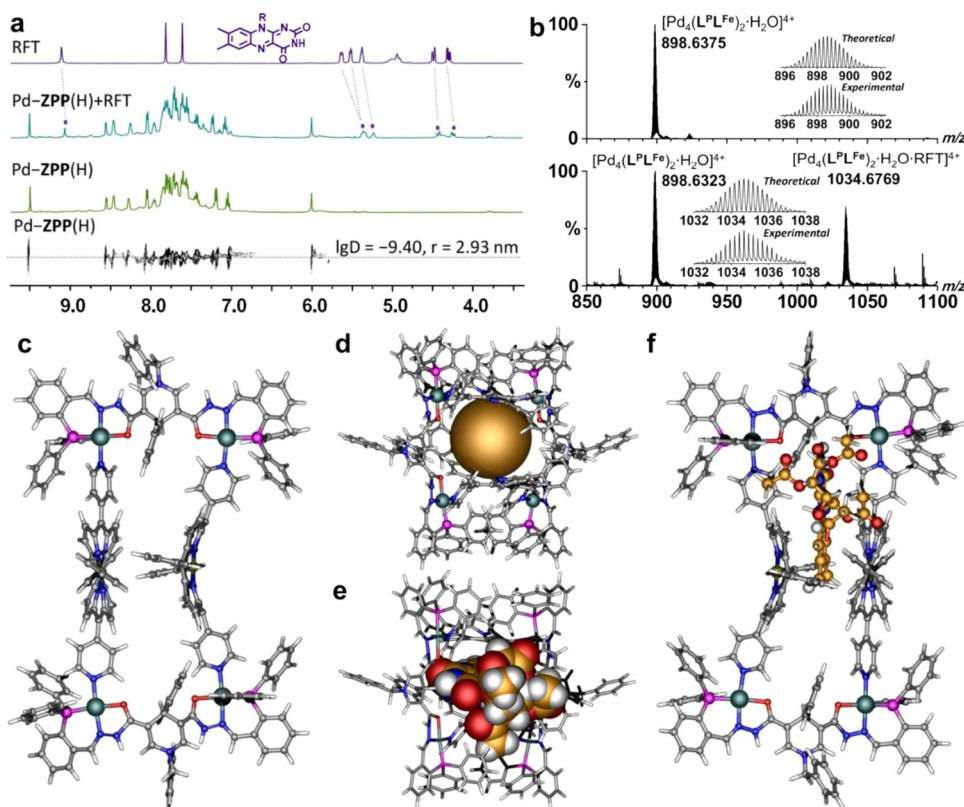


Figure 2. Characterization of macrocycle hosts and host–guest species. (a) Partial ¹H NMR spectra of the metallacycle Pd–ZPP(H) (1.0 mM), RFT (1.0 mM), Pd–ZPP(H) (1.0 mM), and RFT (1.0 mM) mixture in equal concentrations, and ¹H DOSY spectra of Pd–ZPP(H) with log *D* = –9.40 in *d*₆-DMSO. (b) ESI-MS of Pd–ZPP(Fe) (1.0 mM) and the mixture of Pd–ZPP(Fe) (1.0 mM) and RFT (1.0 mM) in DMF; the insets show the measured and simulated isotopic patterns at *m/z* = 898.6375 and 1034.6769, respectively. (c) Structure of the macrocycle Pd–ZPP(Fe) optimized using the PM6 semiempirical method, showing the distribution of the NADH-mimicking sites and porphyrin groups and the square coordination geometry of palladium ions. (d) Resulting beleaguered confined space of Pd–ZPP(Fe). Pd dark green, Fe orange, P wine, O red, N blue, C gray, and H white. (e) and (f) Docking study optimized model of Pd–ZPP(Fe) ⊃ RFT, representing the location of RFT in Pd–ZPP(Fe)’s cavity to meet the close proximity between NADH, flavin, and porphyrin models.

displayed in the ¹H NMR spectrum (Figure S18).³⁸ However, the coordination of ligands to metal ions was indicated by the multinuclear NMR spectra of Pd–ZPP(H). ¹H NMR spectra of Pd–ZPP(H) included the characteristic peaks of both ligand H₂L^P and L^H, and these signals exhibited obvious shifts compared to free ligands; specifically, the imine proton C(O)–NH signal at 11.26 ppm that disappeared compared to ligand H₂L^P was probably due to self-assembly (Figures 2a and S13).¹⁷ The diffusion-ordered NMR spectrum intuitively confirmed the formation of a sole species with a diffusion coefficient of $4.0 \times 10^{-10} \text{ m}^2 \cdot \text{s}^{-1}$ and an estimated diameter of 29.30 Å based on the Stokes–Einstein equation (Figures 2a and S14).^{39,40} Moreover, ³¹P NMR spectrum of Pd–ZPP(H) exhibited singlets at 31.50 ppm with respect to a single phosphorus environment in sharp contrast with that of ligand H₂L^P at –14.05 ppm, suggesting the coordinated formation of pure discrete constructs with a high symmetry (Figure S15).^{41,42} The electrospray ionization mass spectrometry (ESI-MS) analysis of Pd–ZPP(Fe) exhibited an intense peak at *m/z* = 898.6375 assigned to [Pd₄(L^PL^{Fe})₂·H₂O]⁴⁺ via a comparison with the simulation result based on natural isotopic abundances (Figures 2b and S11), while the expected isotopic pattern of [Pd₄(L^PL^H)₂]⁴⁺ species was at *m/z* = 867.6761 for Pd–ZPP(H) in the DMF solution (Figure S12). Both capsules were also suitably stable in the water-containing system, which was indicated by the identical ESI-MS outcomes

in CH₃CN/H₂O (1:1). Moreover, UV–vis absorption and fluorescence spectra of Pd–ZPP(Fe) and Pd–ZPP(H) contained the characteristic peaks of porphyrin and ligand H₂L^P, and no observable change in the emission bands of both Pd–ZPP(Fe) and Pd–ZPP(H) compared to each monomeric ligand suggested that the conjugated effects of both divergent ligands were separated by palladium ions, forming relatively isolated molecular fragments to maintain the intrinsic property of each ligand (Figures S19 and S21).⁴³ These results showcased the realization of paradigmatic structural creation by the careful orchestration of 3:1 complementary coordination between two divergent ligands and square-coordinated ions for self-assembled three-component capsules with high stability.

The optimal geometrical structures by theoretical calculations showed that the compound Pd–ZPP(Fe) was a tetranuclear molecular rectangle containing two divergent ligands.⁴¹ The structure of Pd–ZPP(Fe) was formed by the alternating connection of two ligand H₂L^P containing the central NADH active mimic fragments and two Fe(III)-porphyrin modified ligand L^{Fe} with four palladium ions, producing a pseudo *S*₂-symmetry tetracyclic architecture with a well-defined square channels possessing a ca. 18.83 × 9.43 Å opening, which was sufficiently large to encapsulate RFT (ca. 7.70 Å) into its hydrophobic cavity, ensuring a close proximity between cofactors NADH, flavin modules, and porphyrin

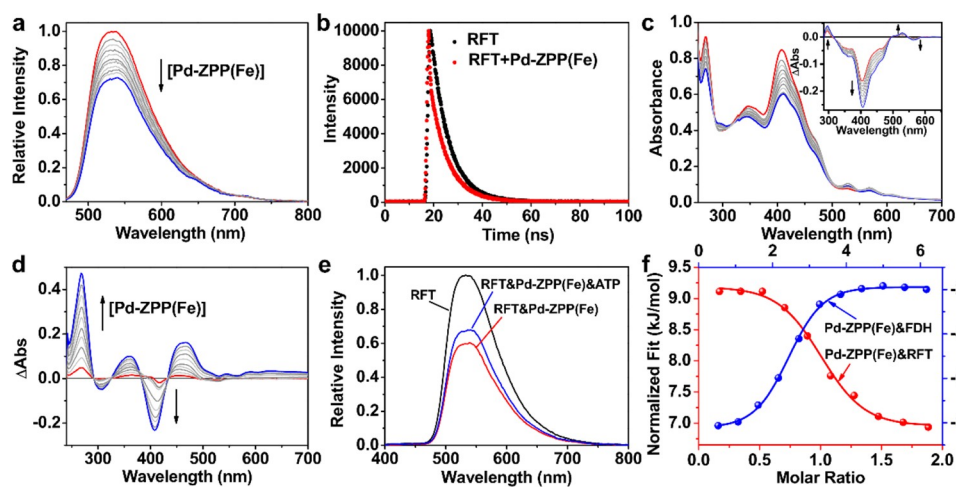


Figure 3. Characterization of the interactions between Pd-ZPP(Fe) and RFT. (a) Luminescence spectra of RFT (10.0 μM) upon the addition of Pd-ZPP(Fe) (7.5 μM) in $\text{CH}_3\text{CN}/\text{H}_2\text{O}$ (1:1). (b) Luminescence decay of RFT (10.0 μM) in CH_3CN and of the aforementioned solution upon the addition of Pd-ZPP(Fe) (10.0 μM). (c) UV-vis spectra of Pd-ZPP(Fe) (10.0 μM) and RFT (10.0 μM) in CH_3CN under 455 nm. Inset shows the differential spectra as a function of irradiation time. (d) Differential UV-vis absorption spectra of Pd-ZPP(Fe) (10.0 μM) in $\text{CH}_3\text{CN}/\text{H}_2\text{O}$ (1:1) upon the addition of RFT (total 10.0 μM). (e) Luminescence spectra of RFT (10.0 μM) in $\text{CH}_3\text{CN}/\text{H}_2\text{O}$ (1:1) upon the addition of Pd-ZPP(Fe) (10.0 μM) and ATP (50.0 μM). (f) ITC experiments of Pd-ZPP(Fe) upon the addition of RFT and of FDH in the $\text{CH}_3\text{CN}/\text{H}_2\text{O}$ (1:1) solution.

active sites (Figures 2c, d; S5). Each palladium ion in Pd-ZPP(Fe) offered a square coordination geometry and was chelated by both the NOP tridentate chelator from ligand $\text{H}_2\text{L}^{\text{P}}$ and the N monodentate chelator from ligand L^{Fe} , which promised all coordinated atoms in one plane.⁴⁴ The divergent ligands cross-distributed on the capsule, where two NADH models or porphyrin units on the opposite side were positioned parallelly on the capsule walls, keeping functional components evenly distributed on the artificial host. Of note, all the active H atoms on the NADH models pointed toward the interior of capsules, which was beneficial to the hydride transfer between the NADH models and Pd-ZPP(Fe)-included RFT to produce the semiquinone form of RFT for further electron conduction to Fe(III)-porphyrin active sites and the activation of molecule oxygen.⁴⁵ Meanwhile, the distribution of NADH mimics on the Pd-ZPP(Fe) surface worked as communicators to connect abiotic and biotic catalysis, ensuring a smooth exchange of protons and electrons within catalytic cycles.¹⁷

Similarly, molecular simulations displayed a similar structure for Pd-ZPP(H) to that of Pd-ZPP(Fe), albeit with differing porphyrin ligands. This advanced fabrication protocol for constructing heteroleptic capsule availably avoided the non-statistical integration of divergent ligands,⁴⁶ and the directionality and angularity of each subunit involved in the coordination-driven self-assembly directed the final pure architectural outcome bearing confined space and functional handles, posing a great opportunity for fabricating cytochrome P450 analogue by encapsulating the flavin moiety.

Host-Guest Interactions and Oxidative Conversions

Theoretical docking calculations suggested that the artificial host Pd-ZPP(Fe) possessed a well-matched opening for the inclusion of guest to form host-guest species Pd-ZPP(Fe) \supset RFT (Figure 2e, f).¹⁸ The aromatic plane of RFT fell within the host cavity, and the aromatic plane was held snugly with the conjugate plane of porphyrin units by efficient aromatic stacking interactions (ca. 3.30 Å), whilst widespread hydrogen-bonding sites on Pd-ZPP(Fe) played an auxiliary role in

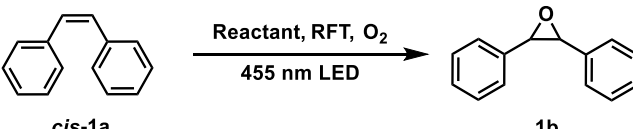
trapping RFT, forming a sandwich supramolecular structure with a calculated ΔG of $-35.03 \text{ kJ}\cdot\text{mol}^{-1}$ (Figure S6).⁴⁷ To the best of our knowledge, it was the first example for mimicking cytochrome P450s by integrating all functional composition within one assembly.^{48,49} In this situation, the flavin analogue was in close proximity to both active sites of NADH and heme models, and the fixed staggered distribution of NADH and heme models subtly improved the synergy and compatibility between individual catalytic components through the bridging of a flavin translocator, which might be beneficial to strengthening the sequential electron transfer chain for catalytic cascade conversions.

The addition of Pd-ZPP(Fe) into RFT solution resulted in an apparent quenching of the emission at 535 nm (Figure 3a). Meanwhile, the luminescence decay of the mixture of RFT and Pd-ZPP(Fe) at 535 nm followed bi-exponential function (Figure 3b), and the lifetime 7.18 ns of the system was able to be divided into 0.43 ns (in 2.69%) and 7.15 ns (in 97.31%), respectively, consistent with the free Pd-ZPP(Fe) lifetime 0.65 ns and free RFT lifetime 7.15 ns (Figure S24). These results indicated that both RFT and Pd-ZPP(Fe) could be activated by light for redox events.⁵⁰ Irradiation of a deaerated $\text{DMSO}-d_6$ solution containing Pd-ZPP(H) (1.0 mM) and RFT (1.0 mM); ^1H NMR spectra showed the emergence of several new peaks at approximately 6.33, 6.41, 10.60, and 10.80 ppm, which were reasonably assigned to RFTH_2 (Figure S17).⁵¹ Moreover, UV-vis spectra of Pd-ZPP(Fe) (10.0 μM) and RFT (10.0 μM) displayed a diminishing intensity at 358 nm assigned to the NADH model with an increasing intensity at 296 nm assigned to the NAD^+ form over irradiation time, indicating that proton and electron transfer could occur from the NADH module on capsule to the excited RFT* upon irradiation (Figure 3c).^{17,52} Furthermore, the absorption at 406 and 432 nm assignable to ligand L^{Fe} and RFT, respectively, decreased gradually accompanied with a weak but obvious change of the Q band belonging to porphyrin groups in the range of 500 to 700 nm, which could be reasonably attributed to the occurrence of a directed electron transfer from the

NADH module via RFT to the Fe(III)-porphyrin site, resembling the electron transfer processes within cytochrome P450s.

The most studied oxidation of alkene derivatives was selected as the benchmark reaction for this study. Irradiation of a DMF solution containing Pd–ZPP(Fe) (1.0 mM), RFT (1.0 mM), and *cis*-stilbene (*cis*-1a, 2.0 mM) in the presence of oxygen for 12 h resulted in a yield of approximately 80% product stilbene oxide (1b) (Table 1, entry 1). Notably,

Table 1. Oxidation of *cis*-Stilbene by Different Reactants with Oxygen^a



entry	reactant	loading (mM)	RFT (mM)	oxidant	yield (%)
1	Pd–ZPP(Fe)	1.0	1.0	O ₂	80 (2)
2	ligand H ₂ L ^P	2.0	1.0	O ₂	trace
3	ligand L ^{Fe}	2.0	1.0	O ₂	trace
4	Pd–ZPP(H)	1.0	1.0	O ₂	trace
5	—	—	1.0	O ₂	trace
6	Pd–ZPP(Fe)	1.0	—	O ₂	trace
7	Pd–ZPP(Fe)	1.0	1.0	—	trace
8 ^b	Pd–ZPP(Fe)	1.0	1.0	O ₂	trace
9 ^c	Pd–ZPP(Fe)	1.0	1.0	O ₂	<15

^aReaction conditions: *cis*-1a (2.0 mM), 455 nm LED, DMF, 37 °C, 12 h. ^bWithout light. ^cIn the presence of inhibitor ATP (2.0 mM). The yields were determined by the gas chromatography analysis of the products with error margins shown in parentheses.

monoligands or nonmetallic porphyrin containing capsule Pd–ZPP(H), as alternatives to Pd–ZPP(Fe), was not able to insert oxygen atoms into the substrate *cis*-1a under the same conditions (Table 1, entries 2–4), indicating that both NADH models and Fe(III)-porphyrin units on metal–organic

architecture Pd–ZPP(Fe) were indispensable catalytic elements in completing oxygenation, and iron porphyrin served as the active site for substrate conversion, which were verified by the chemo-catalysis with oxidants iodosobenzene and iodobenzene diacetate (Table S3).⁵³ Control experiments demonstrated that the absence of either RFT or NADH and heme models comodified Pd–ZPP(Fe) led only isomerization products at the same reaction condition even if oxygen was present, which showed that both RFT and Pd–ZPP(Fe) could sensitize the alkenes under irradiation, and the singlet oxygen that might be present in these reaction conditions was not able to drive oxidation of substrates, indicating the cofactor role of flavin RFT (Table 1, entries 5 and 6).^{54,55} Furthermore, when either oxygen or light was absent, oxidation products could not be detected, indicating that oxygen was the direct oxidant of the reactions and that light promoted the exchange of protons and electrons between cofactors (Table 1, entries 7 and 8).³⁵ In addition, the nonreactive species adenosine triphosphate (ATP, 2.0 mM)⁵⁶ as the inhibitor for competing to occupy the cavity of Pd–ZPP(Fe) was added to a solution containing Pd–ZPP(Fe) (1.0 mM) and RFT (1.0 mM), giving a much lower yield under the same reaction conditions (Table 1, entry 9). The competitive inhibition behavior suggested that the reactions occurred within the pocket of Pd–ZPP(Fe) using oxygen as the oxidant, mimicking cytochrome P450s via encapsulating RFT to drive oxidative conversions.

The formation of host–guest complexation species was further validated for suggesting the pronounced integration of functional components. The addition of RFT (1.0 mM) into a solution of Pd–ZPP(Fe) (1.0 mM) triggered the emergency of a new peak at $m/z = 1034.6769$ assigned to the 1:1 host–guest species $[\text{Pd}_4(\text{L}^{\text{P}}\text{L}^{\text{Fe}})_2\cdot\text{H}_2\text{O}\cdot\text{RFT}]^{4+}$ in the ESI-MS spectrum (Figure 2b). This result could be reflected by the several isosbestic points appeared in the absorption band when adding RFT (10.0 μM) into a CH₃CN/H₂O (1:1) solution of Pd–ZPP(Fe) (10.0 μM) (Figures 3d and S22).⁵⁷ Moreover, the addition of ATP (50.0 μM) into a solution containing RFT

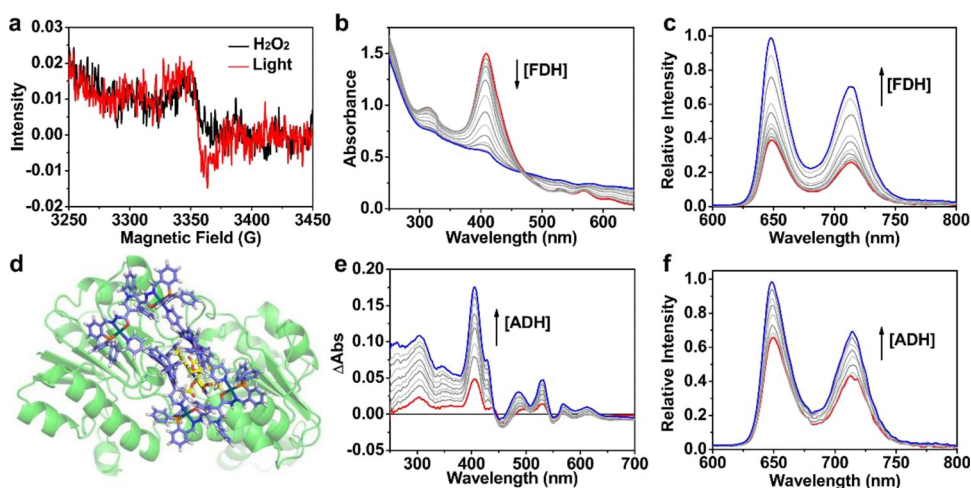


Figure 4. Characterization of the interactions between Pd–ZPP(Fe) and RFT or enzymes. (a) EPR spectra collected at 150 K for the system containing Pd–ZPP(Fe) (1.0 mM) treating with H₂O₂ (10.0 mM) or RFT (1.0 mM) upon the irradiation of xenon lamp in DMF/H₂O (1:1). (b) UV–vis absorption spectra of Pd–ZPP(Fe) (10.0 μM) upon the addition of FDH (total 0.5 μM) in CH₃CN/H₂O (1:1). (c) Family of luminescence spectra of Pd–ZPP(Fe) (10.0 μM) upon the addition of FDH (total 0.5 μM) in CH₃CN/H₂O (1:1). (d) Theoretical docking study optimized model of Pd–ZPP(Fe) ⊃ RFT with enzyme FDH. (e) Differential UV–vis absorption spectra of Pd–ZPP(Fe) (10.0 μM) upon the addition of enzyme ADH (total 0.1 μM) in CH₃CN/H₂O (1:1). (f) Family of luminescence spectra of Pd–ZPP(Fe) (10.0 μM) in CH₃CN/H₂O (1:1) upon the addition of ADH (total 1.0 μM).

(10.0 μM) and Pd-ZPP(Fe) (10.0 μM) resulted in the recovery of RFT emission (Figures 3e and S26), while there was no effect on the emission of RFT (10.0 μM) after the addition of ATP (50.0 μM).¹⁷ These results indicated that RFT was encapsulated in the Pd-ZPP(Fe) pocket, and ATP was capable of extruding RFT out of the capsule pocket (Figure S25), blocking the electron transfer chain and hampering the catalysis within the artificial host. Isothermal titration calorimetry (ITC) experiments showed that upon the addition of RFT to the solution of Pd-ZPP(Fe) gave an association constant of $K_a = 1.05 \times 10^5 \text{ M}^{-1}$ for the complex Pd-ZPP(Fe) \supset RFT with a Gibbs free energy change of $\Delta G = -28.65 \text{ kJ}\cdot\text{mol}^{-1}$ and considerable entropic contribution (Figures 3f and S33), allowing the reproduction of cytochrome P450s catalysis accompanied with the activation of binding.^{58,59} These results indicated that the spontaneous molecular binding behavior between host and guest molecules ensured the inclusion of RFT by both NADH and heme models comodified capsule Pd-ZPP(Fe) with appreciable affinity, shortening the distance between cofactors and Fe(III)-porphyrin active sites and spatially permitting the electron transfer between them. On this basis, the activation of oxygen by Fe(III)-porphyrin was further verified by electron paramagnetic resonance (EPR) spectra. The EPR measurements under air revealed a characteristic signal with a g value of 2.006 because of the generation of Fe(IV)-oxo active species after irradiating the mixture of Pd-ZPP(Fe) (1.0 mM) and RFT (1.0 mM), consistent with the response when Pd-ZPP(Fe) (1.0 mM) was treated with hydrogen peroxide (Figure 4a), which was in line with previously reported EPR spectra of the ferryl species raised in natural cytochrome P450 oxygenase.⁶⁰ In contrast, light-irradiating the solution containing both Pd-ZPP(H) (1.0 mM) and RFT (1.0 mM) led to a failure in producing the signal response of such active species, which was responsible for the inability to complete oxidation (Table 1, entry 4) despite 1:1 binding host-guest species formed as indicated by the shift of peaks attributable to RFT in ^1H NMR spectra (Figures 2a and S16), the ESI-MS peak at $m/z = 1003.7198$ belonging to $[\text{Pd}_4(\text{L}^{\text{PLH}})_2\cdot(\text{RFT})]^{4+}$ (Figure S12), and isosbestic points presented in UV-vis spectra (Figure S23).

Hence, the catalysis by artificial cytochrome P450 Pd-ZPP(Fe) was initiated by an electron originating from an NADH analogue on the surface of the capsule through the reduced form of the flavin cofactor to the Fe(III)-porphyrin unit within capsule cavity. The electron-derived heme group transferred the surplus electrons to molecular oxygen in a spin-matching way to produce ferric superoxo species, which was intuitively diagnosed by the α -terpinene oxidation test for the emergency of the p -cymene-based product.⁶¹ The oxygen-binding porphyrin then underwent the generation of different forms of reactive oxygen species, affording ferric peroxide adducts for inducing inactive C-H bond oxidation inside the capsule.²²⁻²⁴ Without the regeneration of the NADH mimics, these cofactors just worked as stoichiometric reactants to feed the oxygenation reactions. Interestingly, following studies unexpectedly showed that when additional typical enzymatic substrates (such as formate and alcohol) were added to the reaction system, the product **1b** formed by mimicking cytochrome P450 catalysis was further transformed into oxidative coupling products (2-oxo-1,2-diphenylethyl formate, **1c**; 2-ethoxy-1,2-diphenylethanolone, **1d**) with high selectivity and efficacy (Table S4), which might attribute to the reaction

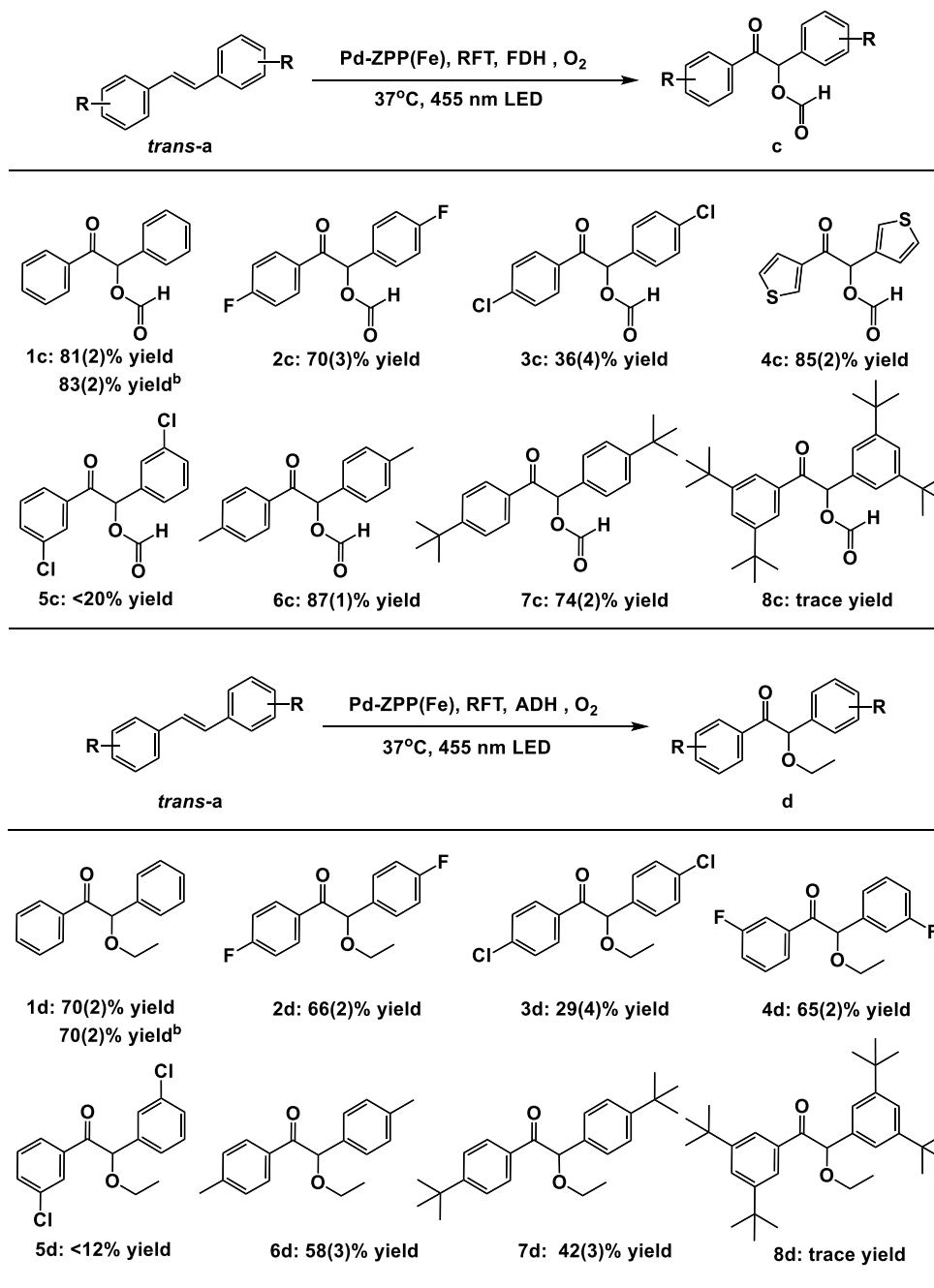
of artificial catalytic outcome **1b** and enzymatic nucleophilic substrates.⁶²⁻⁶⁴ This represented a rare example to complete catalytic conversions of both intrinsic and extrinsic reactions by one artificial cytochrome P450 enzyme. These results indicated that the artificial system could combine with different enzymes to obtain divergent coupled catalytic products, which was promised by the confinement effects of capsules to separate redox events,⁶⁵ and the distribution of NADH mimics on the surface of capsules to directly couple natural enzymatic systems.

Tandem Catalysis by Artificial and Natural Enzymes

The supramolecular catalysis driven by artificial capsule Pd-ZPP(Fe) was supposed to be able to combine with enzymatic catalysis on account of the individual microenvironment for limiting catalysis and the NADH mimics located on the surface of capsules for proton and electron transporting. It was considered that the affinity and compatibility between the cofactor itself and the enzyme protein would facilitate the combination of cofactor-modified artificial catalysts and natural catalysts.^{66,67}

Therefore, the host-guest relationship between the artificial host and natural enzyme was first considered. The ITC assay of Pd-ZPP(Fe) upon the addition of formate dehydrogenase (FDH) gave an association constant $K_a = 3.98 \times 10^6 \text{ M}^{-1}$ with a good fitting of the experimental isotherms, wherein a large change in ΔG was calculated as $-36.42 \text{ kJ}\cdot\text{mol}^{-1}$, reflecting the considerable affinity between the natural host FDH and Pd-ZPP(Fe) and the generation of host-guest species by noncovalent interactions (Figures 3f and S34).^{17,68} Inductively coupled plasma-optical emission spectroscopy (ICP-OES) analysis of the solid mixture of Pd-ZPP(Fe)/FDH showed a 2:1 binding ratio between Pd-ZPP(Fe) and FDH in the combined system, consistent with the result from ITC assay (Table S1). The binding event between artificial and natural catalysts was verified by the emerged isosbestic points at 470 nm in the UV-vis absorption spectra when adding FDH (total 0.5 μM) to Pd-ZPP(Fe) (10.0 μM) (Figures 4b and S28).^{17,69} An enhanced luminescence of Pd-ZPP(Fe) (10.0 μM) appeared at both 648 and 714 nm upon the addition of FDH (total 0.5 μM) (Figure 4c).⁷⁰ Notably, this spectra revealed significant changes from an initial linear growth to almost unchanged (Figure S27), which could be interpreted as the steady binding between Pd-ZPP(Fe) and enzyme FDH arising from recognition between them.^{18,71} Importantly, circular dichroism and luminescence spectra showed that the characteristic peaks attributable to FDH were basically maintained after adding the capsule Pd-ZPP(Fe) and prolonging time, suggesting the stability of the combined system with the secondary and tertiary structures of FDH preserved (Figures S30-S32).

Theoretical docking study in random binding mode further revealed that the RFT-containing heteroleptic capsule was capable of binding to the FDH catalytic pocket to form one working module and produce a transparent channel with FDH opening, which allowed the exchange of substrates between artificial and natural enzymes (Figures 4d and S7).^{18,72} In this case, the capsule binding to the FDH catalytic pocket was the major binding conformation with the binding energy calculated as $-34.99 \text{ kJ}\cdot\text{mol}^{-1}$ (Figure S8), which was in line with the binding energy provided by ITC assay. The high-affinity binding might benefit from the suitable opening and electrostatic and noncovalent interaction sites of the enzymatic

Table 2. Oxidative Coupling Reactions Driven by Pd–ZPP(Fe) with Different Enzymes^{a,b}

^aFor the system with FDH: substrate (8.0 mM), Pd–ZPP(Fe) (1.0 mM), RFT (1.0 mM), FDH (1.0 U·mL⁻¹), and HCOONa (24.0 mM) in a CH₃CN/H₂O (1:1) solution, 455 nm LED, 12 h. For the system with ADH: substrate (8.0 mM), Pd–ZPP(Fe) (1.0 mM), RFT (1.0 mM), ADH (10.0 U·mL⁻¹) in a CH₃CN/CH₃CH₂OH/H₂O (1:1:1) solution, 455 nm LED, 12 h. Yields were determined by the gas chromatography analysis of the products with error margins shown in parentheses. ^bSubstrate was replaced by *cis*-1a (8.0 mM).

pocket. Therefore, we anticipated that Pd–ZPP(Fe) was able to attach to FDH, which allowed it to directly participate in enzymatic reactions for cascade catalysis.

The tandem catalysis was first exploited in a CH₃CN/H₂O (1:1) solution containing substrate *cis*-1a (8.0 mM), Pd–ZPP(Fe) (1.0 mM), RFT (1.0 mM), FDH (1.0 U·mL⁻¹), and HCOONa (24.0 mM) upon 455 nm light. This catalytic system only produced a trace amount of monooxygenation product 1b but formed an 83% yield of the oxidative coupling product 1c (Table 2, with substrate *cis*-1a) with the ESI-MS signal assigned to Pd–ZPP(Fe) maintained. The catalytic

amount of Pd–ZPP(Fe) to achieve efficient conversions was ascribed to the direct regeneration of the consumed NADH mimics in situ by enzymatic dehydrogenations in one working microenvironment,¹⁷ and the supramolecular catalytic product could further interact with the enzymatic nucleophilic substrate within the enzymatic domain directly affording cascade products. Moreover, the combined system displayed a pseudo-zero-order kinetic behavior during the initial stage of reactions, and the initial kinetics generally satisfied a Lineweaver–Burk plot with the concentration of substrates (Figures S36 and S37), further inferring that the capsule was

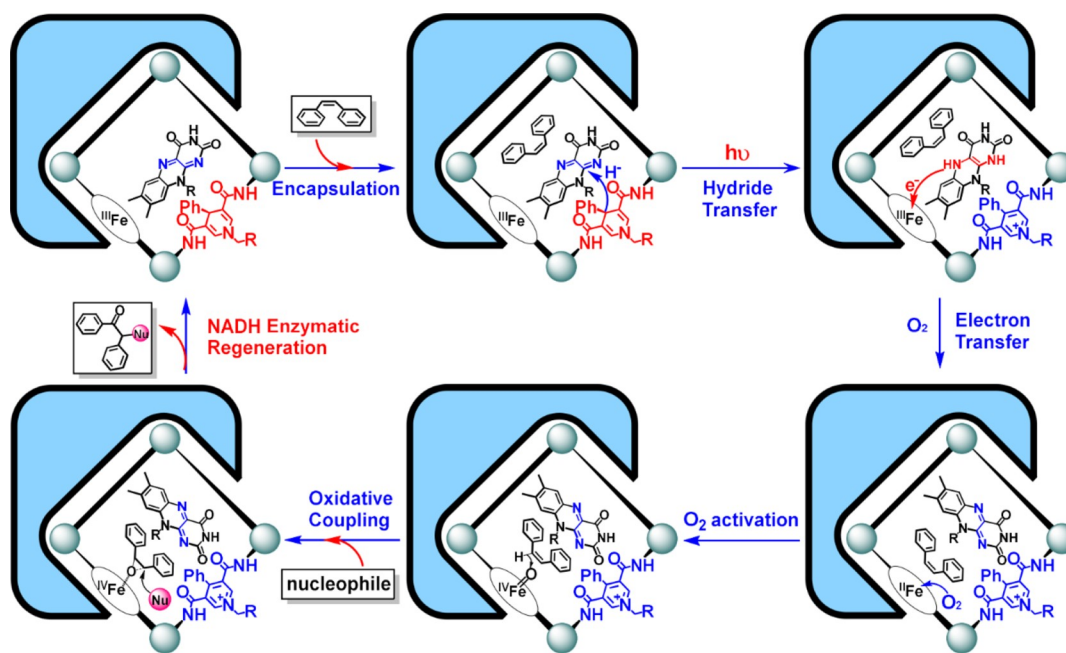


Figure 5. Schematic of the supramolecular catalytic oxidation of *cis*-stilbene, showing the synergistic catalytic behavior of artificial and natural enzymes within the confined environment and in situ regeneration of the NADH model under enzymatic catalysis.

bound to FDH and served as a combined catalyst, and multistep reactions occurred inside the capsule. This catalytic mode masterly simulated the natural catalysis and avoided the use of additional agents, promoting a circulating catalysis with a closed loop of electrons and protons.

This oxidative coupling catalysis could further expand from *cis*-alkenes to *trans*-alkenes (Table 2), which might be due to the photosensitizing effect of flavin and the elimination of restrictions imposed by the stereo configuration.^{53,73} Moreover, we found that regardless of the substrate steric hindrance effect, the yields of electron-withdrawing substituent-modified substrates decreased as the substituent constant increased (Table 2, with substrate *trans*-2a and 3a). Even the reactant coming to a bromine-modified substrate could not afford the relevant target. These results indicated that the essence of the coupling process was a nucleophilic addition reaction, and electron-rich substrates deserved a better result. When the experiment performed with a *trans*-alkene containing multiple sterically hindered substituents (Table 2, with substrate *trans*-8a), little coupling product was produced under the same reaction conditions. The oxygenation reaction constrained by the pocket of Pd-ZPP(Fe) was further verified by the experiment with inhibitor ATP (2.0 mM) and afforded a 14% yield of 1c in the optimal condition.

The attempt to hybridize the biological enzyme by Pd-ZPP(Fe) was further extended to alcohol dehydrogenase (ADH). The addition of ADH (total 0.1 μM) into a solution containing Pd-ZPP(Fe) (10.0 μM) resulted in an isosbestic point in the absorption band at 442 nm (Figures 4e and S29) and caused similar emission enhancement at 648 and 714 nm to the Pd-ZPP(Fe)/FDH system (Figure 4f), confirming that Pd-ZPP(Fe) could assemble an integrated suprastructure with ADH in like manner when encountered in an ADH microenvironment. ITC measurements gave a binding constant reaching $1.19 \times 10^6 \text{ M}^{-1}$ between Pd-ZPP(Fe) and ADH with a ΔG of $-34.68 \text{ kJ}\cdot\text{mol}^{-1}$ (Figure S35), being highly consistent with that ($-34.48 \text{ kJ}\cdot\text{mol}^{-1}$) provided by

theoretical docking experiments where the capsule Pd-ZPP(Fe) majorly bound to the crack of the ADH catalytic pocket through noncovalent interactions (Figures S9 and S10), suggesting that the semibiological system consisting of Pd-ZPP(Fe) and ADH might be also competent for cascade catalysis. Therefore, the catalysis was then performed with ADH (10.0 $\text{U}\cdot\text{mL}^{-1}$), Pd-ZPP(Fe) (1.0 mM), RFT (1.0 mM), and substrate *cis*-1a (8.0 mM) in a $\text{CH}_3\text{CN}/\text{CH}_3\text{CH}_2\text{OH}/\text{H}_2\text{O}$ (1:1:1) solution. It was gratifying that the catalysis with ADH gave oxidative coupling product 1d in 70% yield (Table 2, with substrate *cis*-1a). The superiority of such cascade systems could be extended to *trans*-stilbene with different substituents, which also showed the influence of the substituent effect on the cascade reactions (Table 2). However, it was noted that the weaker nucleophilicity of $\text{CH}_3\text{CH}_2\text{OH}$ compared to HCOONa required a large amount of ethanol to drive catalysis. As ADH is also active with branched chain alcohols and secondary alcohols,⁷⁴ we further employed methanol and isopropanol as both enzymatic substrates in the tandem system and exactly found that 60% yield of 2-methoxy-1,2-diphenylethanone and 24% yield of 2-isopropoxy-1,2-diphenylethanone were able to be obtained by the oxidative coupling of *trans*-stilbene with methanol and isopropanol, respectively, under similar conditions (Table S5). In general, excessive nucleophiles were not only the substrate of oxidative coupling cascade catalysis but served as enzymatic substrates to regenerate the consumed NADH models in the artificial catalysis. These catalytic results suggested the broad biocompatibility of Pd-ZPP(Fe) to combine established enzymes for non-native catalysis, resembling the different metabolic pathways in those living organisms for achieving different purposes.

From a mechanistic viewpoint, through the careful orchestration of the flavin unit encapsulated by a NADH and heme mimics comodified heteroleptic metal-organic capsule for inclusion into the dehydrogenase catalytic pocket in a matryoshka fashion, a new supramolecular host-guest semi-

biological system was well fabricated to simultaneously combine a biomimetic cytochrome P450s catalysis with a NADH-regenerated biotic catalysis within the pocket of enzymes, allowing bio-orthogonal catalysis for cascade reactions (Figure 5). The well-modified artificial metal–organic host that integrated all functional compositions of cytochrome P450s within one assembly effectively shortened the distance between NADH, flavin, and heme mimics, which could restrain a pseudo-intramolecular electron transfer chain from the NADH cofactor via the flavin cofactor to the porphyrin catalytic site, which originally occurred in cytochrome P450s, inside the capsule pocket, and immobilized the electron flow for a strengthened electron and energy transport. Molecular oxygen completed the conversion at the electron-rich heme site through the reductive activation path and finally generated reactive ferric peroxide species for C–H oxidation.

The allosteric regulation enzymes in response to the binding of the capsule might allow this abiotic catalytic system to be further embedded into different enzyme pockets to couple divergent enzymatic nucleophilic substrates for oxidative coupling products, meanwhile, combine enzymatic dehydrogenation to regenerate the consumed NADH in situ through transient collisions for achieving multiple turnovers.⁷⁵ This host–guest approach to joining artificial and enzymatic catalysis allowed a direct modification of multiple exogenous catalytic sites into the catalytic domain of natural enzymes, and the formed closed range between artificial and natural catalytic sites enhanced the transfer of matter and energy at the same location, enabling smooth switching between two catalytic cycles and avoiding the diffusion and expense of co-enzymes. The inherent confined effects and secondary coordination sphere effects by both artificial and natural hosts achieved the optimized allocation of matter and energy by creating regional cooperation and division, which was in favor of controlling electron transfer pathways and altering the performance of catalysis, eliminating inherent mutual interferences between the artificial and natural catalysis and promoting the formation of a circulating catalytic system for one-pot integrated catalytic conversions.

CONCLUSIONS

In summary, a heteroleptic metal–organic capsule Pd–ZPP(Fe) as a cytochrome P450s analogue was developed and embedded into enzymatic pockets in a host–guest approach for multistep C–H oxidative coupling catalysis. The elaborate integration of functional units (nicotinamide- and flavin-based cofactors, porphyrin catalytic site) in a working module not only promises the immobilization of electron flow that occurs inside the capsule for the effective reductive activation of oxygen and the strengthened delivery of matters and energy but also allows the direct proton and electron transportation via NADH channels on the capsule surface. This host–guest approach to simultaneously introduce divergent functional groups into different enzymes promises parallel reactions for divergent catalytic results, providing a distinguished mean to achieve ideal levels of resource economy in cascade syntheses for developing scalable and sustainable bidirectional catalysis involving multiple active sites, environmental benign redox reagents, renewable feedstock, and even exogenous metal catalytic sites.

ASSOCIATED CONTENT

Supporting Information

The Supporting Information is available free of charge at <https://pubs.acs.org/doi/10.1021/jacsau.2c00322>.

Experimental as well as synthetic procedures and further spectroscopic and analytical data, and details of the theoretical calculations (PDF)

AUTHOR INFORMATION

Corresponding Authors

Liang Zhao – State Key Laboratory of Fine Chemicals, Zhang Dayu School of Chemistry, Dalian University of Technology, Dalian 116024, People's Republic of China; orcid.org/0000-0001-8197-6686; Email: zhaol@dlut.edu.cn

Chunying Duan – State Key Laboratory of Fine Chemicals, Zhang Dayu School of Chemistry, Dalian University of Technology, Dalian 116024, People's Republic of China; State Key Laboratory of Coordination Chemistry, Nanjing University, Nanjing 210023, People's Republic of China; orcid.org/0000-0003-1638-6633; Email: cyduan@dlut.edu.cn

Authors

Junkai Cai – State Key Laboratory of Fine Chemicals, Zhang Dayu School of Chemistry, Dalian University of Technology, Dalian 116024, People's Republic of China; State Key Laboratory of Coordination Chemistry, Nanjing University, Nanjing 210023, People's Republic of China

Yanan Li – State Key Laboratory of Fine Chemicals, Zhang Dayu School of Chemistry, Dalian University of Technology, Dalian 116024, People's Republic of China

Cheng He – State Key Laboratory of Fine Chemicals, Zhang Dayu School of Chemistry, Dalian University of Technology, Dalian 116024, People's Republic of China; orcid.org/0000-0002-1426-0124

Chong Wang – State Key Laboratory of Fine Chemicals, Zhang Dayu School of Chemistry, Dalian University of Technology, Dalian 116024, People's Republic of China

Complete contact information is available at: <https://pubs.acs.org/doi/10.1021/jacsau.2c00322>

Notes

The authors declare no competing financial interest.

ACKNOWLEDGMENTS

This work was supported by the National Natural Science Foundation of China (Nos. 22171034, 21820102001, and 21890381) and the Fundamental Research Funds for the Central Universities (DUT20TD101).

REFERENCES

- (1) Leveson-Gower, R. B.; Mayer, C.; Roelfes, G. The Importance of Catalytic Promiscuity for Enzyme Design and Evolution. *Nat. Rev. Chem.* **2019**, *3*, 687–705.
- (2) Lewis, J. C. Beyond the Second Coordination Sphere: Engineering Dirhodium Artificial Metalloenzymes to Enable Protein Control of Transition Metal Catalysis. *Acc. Chem. Res.* **2019**, *52*, 576–584.
- (3) Chen, K.; Arnold, F. H. Engineering New Catalytic Activities in Enzymes. *Nat. Catal.* **2020**, *3*, 203–213.

- (4) Dhakshinamoorthy, A.; Asiri, A. M.; Garcia, H. Metal–Organic Frameworks as Multifunctional Solid Catalysts. *Trends Chem.* **2020**, *2*, 454–466.
- (5) Dhakshinamoorthy, A.; Asiri, A. M.; Garcia, H. Integration of Metal Organic Frameworks with Enzymes as Multifunctional Solids for Cascade Catalysis. *Dalton Trans.* **2020**, *49*, 11059–11072.
- (6) Dhakshinamoorthy, A.; Garcia, H. Cascade Reactions Catalyzed by Metal Organic Frameworks. *ChemSusChem* **2014**, *7*, 2392–2410.
- (7) Palomo, J. M. Artificial Enzymes with Multiple Active Sites. *Curr. Opin. Green Sustain. Chem.* **2021**, *29*, No. 100452.
- (8) Alonso, S.; Santiago, G.; Cea-Rama, I.; Fernandez-Lopez, L.; Coscolin, C.; Modregger, J.; Ressmann, A. K.; Martínez-Martínez, M.; Marrero, H.; Bargiela, R.; Pita, M.; Gonzalez-Alfonso, J. L.; Briand, M. L.; Rojo, D.; Barbas, C.; Plou, F. J.; Golyshin, P. N.; Shahgaldian, P.; Sanz-Aparicio, J.; Guallar, V.; Ferrer, M. Genetically Engineered Proteins with Two Active Sites for Enhanced Biocatalysis and Synergistic Chemo- and Biocatalysis. *Nat. Catal.* **2020**, *3*, 319–328.
- (9) Li, W.-L.; Head-Gordon, T. Catalytic Principles from Natural Enzymes and Translational Design Strategies for Synthetic Catalysts. *ACS Cent. Sci.* **2021**, *7*, 72–80.
- (10) Wang, Z. J.; Clary, K. N.; Bergman, R. G.; Raymond, K. N.; Toste, F. D. A Supramolecular Approach to Combining Enzymatic and Transition Metal Catalysis. *Nat. Chem.* **2013**, *5*, 100–103.
- (11) Liu, K.; Yuan, C.; Zou, Q.; Xie, Z.; Yan, X. A Self-Assembled Zinc/Cystine-Based Chloroplast Mimics Capable of Photoenzymatic Reactions for Sustainable Fuel Synthesis. *Angew. Chem., Int. Ed.* **2017**, *56*, 7876–7880.
- (12) Sun, Y.; Shi, J.; Wang, Z.; Wang, H.; Zhang, S.; Wu, Y.; Wang, H.; Li, S.; Jiang, Z. Thylakoid Membrane-Inspired Capsules with Fortified Cofactor Shuttling for Enzyme-Photocoupled Catalysis. *J. Am. Chem. Soc.* **2022**, *144*, 4168–4177.
- (13) Walsh, C. T.; Tu, B. P.; Tang, Y. Eight Kinetically Stable but Thermodynamically Activated Molecules That Power Cell Metabolism. *Chem. Rev.* **2018**, *118*, 1460–1494.
- (14) McSkimming, A.; Colbran, S. B. The Coordination Chemistry of Organo-Hydride Donors: New Prospects for Efficient Multi-Electron Reduction. *Chem. Soc. Rev.* **2013**, *42*, 5439–5488.
- (15) Pullen, S.; Clever, G. H. Mixed-Ligand Metal–Organic Frameworks and Heteroleptic Coordination Cages as Multifunctional Scaffolds—A Comparison. *Acc. Chem. Res.* **2018**, *51*, 3052–3064.
- (16) Cook, T. R.; Stang, P. J. Recent Developments in the Preparation and Chemistry of Metallacycles and Metallacages via Coordination. *Chem. Rev.* **2015**, *115*, 7001–7045.
- (17) Zhao, L.; Cai, J.; Li, Y.; Wei, J.; Duan, C. A Host–Guest Approach to Combining Enzymatic and Artificial Catalysis for Catalyzing Biomimetic Monooxygenation. *Nat. Commun.* **2020**, *11*, 2903.
- (18) Cai, J.; Zhao, L.; He, C.; Li, Y.; Duan, C. A Host–Guest Semibiological Photosynthesis System Coupling Artificial and Natural Enzymes for Solar Alcohol Splitting. *Nat. Commun.* **2021**, *12*, 5092.
- (19) Tang, Y.; Wu, H.; Wei, T.; Li, X. Chemical Protein Synthesis: Advances, Challenges, and Outlooks. *J. Am. Chem. Soc.* **2020**, *142*, 20288–20298.
- (20) Cao-Milán, R.; Gopalakrishnan, S.; He, L. D.; Huang, R.; Wang, L.; Castellanos, L.; Luther, D. C.; Landis, R. F.; Makabenta, J. M. V.; Li, C.; Zhang, X.; Scaletti, F.; Vachet, R. W.; Rotello, V. M. Thermally Gated Bio-Orthogonal Nanozymes with Supramolecularly Confined Porphyrin Catalysts for Antimicrobial Uses. *Chem* **2020**, *6*, 1113–1124.
- (21) Dalton, T.; Faber, T.; Glorius, F. C–H Activation: Toward Sustainability and Applications. *ACS Cent. Sci.* **2021**, *7*, 245–261.
- (22) Chakrabarty, S.; Wang, Y.; Perkins, J. C.; Narayan, A. R. H. Scalable Biocatalytic C–H Oxyfunctionalization Reactions. *Chem. Soc. Rev.* **2020**, *49*, 8137–8155.
- (23) Huang, X.; Groves, J. T. Oxygen Activation and Radical Transformations in Heme Proteins and Metalloporphyrins. *Chem. Rev.* **2018**, *118*, 2491–2553.
- (24) Dunham, N. P.; Arnold, F. H. Nature’s Machinery, Repurposed: Expanding the Repertoire of Iron-Dependent Oxygenases. *ACS Catal.* **2020**, *10*, 12239–12255.
- (25) Denisov, I. G.; Makris, T. M.; Sligar, S. G.; Schlichting, I. Structure and Chemistry of Cytochrome P450. *Chem. Rev.* **2005**, *105*, 2253–2278.
- (26) Feiters, M. C.; Rowan, A. E.; Nolte, R. J. M. From Simple to Supramolecular Cytochrome P450 Mimics. *Chem. Soc. Rev.* **2000**, *29*, 375–384.
- (27) Kitagishi, H.; Kano, K. Synthetic Heme Protein Models that Function in Aqueous Solution. *Chem. Commun.* **2021**, *57*, 148–173.
- (28) Wang, M.; Roberts, D. L.; Paschke, R.; Shea, T. M.; Masters, B. S. S.; Kim, J. P. Three-Dimensional Structure of NADPH-Cytochrome P450 Reductase: Prototype for FMN- and FAD-Containing Enzymes. *Proc. Natl. Acad. Sci. U. S. A.* **1997**, *94*, 8411–8416.
- (29) Jin, Y.; Zhang, Q.; Zhang, Y.; Duan, C. Electron Transfer in the Confined Environments of Metal–Organic Coordination Supramolecular Systems. *Chem. Soc. Rev.* **2020**, *49*, 5561–5600.
- (30) Zaffaroni, R.; Bobylev, E. O.; Plessius, R.; van der Vlugt, J. I.; Reek, J. N. H. How to Control the Rate of Heterogeneous Electron Transfer across the Rim of M_6L_{12} and $M_{12}L_{24}$ Nanospheres. *J. Am. Chem. Soc.* **2020**, *142*, 8837–8847.
- (31) Wu, K.; Li, K.; Chen, S.; Hou, Y.; Lu, Y.; Wang, J.; Wei, M.; Pan, M.; Su, C. The Redox Coupling Effect in a Photocatalytic Ru^{II} - Pd^{II} Cage with TTF Guest as Electron Relay Mediator for Visible-Light Hydrogen-Evolving Promotion. *Angew. Chem., Int. Ed.* **2020**, *59*, 2639–2643.
- (32) Lu, Y.; He, C.; Zhang, H.; Jin, G. Molecular Borromean Rings Based on Half-Sandwich Organometallic Rectangles. *Acc. Chem. Res.* **2018**, *51*, 2148–2158.
- (33) Preston, D.; Inglis, A. R.; Garden, A. L.; Kruger, P. E. A Symmetry Interaction Approach to $[M_2L_2]^{4+}$ Metalloclusters and Their Self-Catenation. *Chem. Commun.* **2019**, *55*, 13271–13274.
- (34) Hering, T.; Mühlendorf, B.; Wolf, R.; König, B. Halogenase-Inspired Oxidative Chlorination Using Flavin Photocatalysis. *Angew. Chem., Int. Ed.* **2016**, *55*, 5342–5345.
- (35) Rauch, M.; Schmidt, S.; Arends, I. W. C. E.; Oppelt, K.; Karac, S.; Hollmann, F. Photobiocatalytic Alcohol Oxidation Using LED Light Sources. *Green Chem.* **2017**, *19*, 376–379.
- (36) Cook, T. R.; Zheng, Y.; Stang, P. J. Metal–Organic Frameworks and Self-Assembled Supramolecular Coordination Complexes: Comparing and Contrasting the Design, Synthesis, and Functionality of Metal–Organic Materials. *Chem. Rev.* **2013**, *113*, 734–777.
- (37) Li, H.; Fan, J.; Hu, M.; Cheng, G.; Zhou, D.; Wu, T.; Song, F.; Sun, S.; Duan, C.; Peng, X. Highly Sensitive and Fast-Responsive Fluorescent Chemosensor for Palladium: Reversible Sensing and Visible Recovery. *Chem. – Eur. J.* **2012**, *18*, 12242–12250.
- (38) Chen, J.; Browne, W. R. Photochemistry of Iron Complexes. *Coord. Chem. Rev.* **2018**, *374*, 15–35.
- (39) Avram, L.; Cohen, Y. Diffusion NMR of Molecular Cages and Capsules. *Chem. Soc. Rev.* **2015**, *44*, 586–602.
- (40) Yamashina, M.; Tanaka, Y.; Lavendomme, R.; Ronson, T. K.; Pittelkow, M.; Nitschke, J. R. An Antiaromatic-Walled Nanospace. *Nature* **2019**, *574*, 511–515.
- (41) Yan, X.; Wang, H.; Hauke, C. E.; Cook, T. R.; Wang, M.; Saha, M. L.; Zhou, Z.; Zhang, M.; Li, X.; Huang, F.; Stang, P. J. A Suite of Tetraphenylethylene-Based Discrete Organoplatinum(II) Metallacycles: Controllable Structure and Stoichiometry, Aggregation-Induced Emission, and Nitroaromatics Sensing. *J. Am. Chem. Soc.* **2015**, *137*, 15276–15286.
- (42) Chen, L.; Chen, C.; Sun, Y.; Lu, S.; Huo, H.; Tan, T.; Li, A.; Li, X.; Ungar, G.; Liu, F.; Zhang, M. Luminescent Metallacycle-Cored Liquid Crystals Induced by Metal Coordination. *Angew. Chem., Int. Ed.* **2020**, *59*, 10143–10150.
- (43) Jia, P.; Xu, L.; Hu, Y.; Li, W.; Wang, X.; Ling, Q.; Shi, X.; Yin, G.; Li, X.; Sun, H.; Jiang, Y.; Yang, H. Orthogonal Self-Assembly of a Two-Step Fluorescence-Resonance Energy Transfer System with

Improved Photosensitization Efficiency and Photooxidation Activity. *J. Am. Chem. Soc.* **2021**, *143*, 399–408.

(44) Felton, G. A. N.; Glass, R. S.; Lichtenberger, D. L.; Evans, D. H. Palladium(II) Complexes of Readily Functionalized Bidentate 2-Pyridyl-1,2,3-Triazole “Click” Ligands: A Synthetic, Structural, Spectroscopic, and Computational Study. *Inorg. Chem.* **2011**, *50*, 6334–6346.

(45) Dubey, K. D.; Shaik, S. Choreography of the Reductase and P450_{BM3} Domains Toward Electron Transfer Is Instigated by the Substrate. *J. Am. Chem. Soc.* **2018**, *140*, 683–690.

(46) Yan, L.; Tan, C.; Zhang, G.; Zhou, L.; Bünzli, J.; Sun, Q. Stereocontrolled Self-Assembly and Self-Sorting of Luminescent Europium Tetrahedral Cages. *J. Am. Chem. Soc.* **2015**, *137*, 8550–8555.

(47) Sawada, T.; Yoshizawa, M.; Sato, S.; Fujita, M. Minimal Nucleotide Duplex Formation in Water through Enclathration in Self-Assembled Hosts. *Nat. Chem.* **2009**, *1*, 53–56.

(48) Durot, S.; Taesch, J.; Heitz, V. Multiporphyrinic Cages: Architectures and Functions. *Chem. Rev.* **2014**, *114*, 8542–8578.

(49) Percástegui, E. G.; Jancik, V. Coordination-Driven Assemblies Based on Meso-Substituted Porphyrins: Metal–Organic Cages and a New Type of Meso-Metallaporphyrin Macrocycles. *Coord. Chem. Rev.* **2020**, *407*, No. 213165.

(50) Jing, X.; He, C.; Yang, Y.; Duan, C. A Metal–Organic Tetrahedron as a Redox Vehicle to Encapsulate Organic Dyes for Photocatalytic Proton Reduction. *J. Am. Chem. Soc.* **2015**, *137*, 3967–3974.

(51) Feldmeier, C.; Bartling, H.; Magerl, K.; Gschwind, R. M. LED-Illuminated NMR Studies of Flavin-Catalyzed Photooxidations Reveal Solvent Control of the Electron-Transfer Mechanism. *Angew. Chem., Int. Ed.* **2015**, *54*, 1347–1351.

(52) Freeman, R.; Willner, I. NAD⁺/NADH-Sensitive Quantum Dots: Applications to Probe NAD⁺-Dependent Enzymes and to Sense the RDX Explosive. *Nano Lett.* **2009**, *9*, 322–326.

(53) Kuijpers, P. F.; Otte, M.; Dürr, M.; Ivanović-Burmazović, I.; Reek, J. N. H.; de Bruin, B. A Self-Assembled Molecular Cage for Substrate-Selective Epoxidation Reactions in Aqueous Media. *ACS Catal.* **2016**, *6*, 3106–3112.

(54) Metternich, J. B.; Gilmour, R. One Photocatalyst, *n* Activation Modes Strategy for Cascade Catalysis: Emulating Coumarin Biosynthesis with (–)-Riboflavin. *J. Am. Chem. Soc.* **2016**, *138*, 1040–1045.

(55) Neveselý, T.; Svobodová, E.; Chudoba, J.; Sikorski, M.; Cibulka, R. Efficient Metal-Free Aerobic Photooxidation of Sulfides to Sulfoxides Mediated by a Vitamin B₂ Derivative and Visible Light. *Adv. Synth. Catal.* **2016**, *358*, 1654–1663.

(56) He, C.; Wang, J.; Zhao, L.; Liu, T.; Zhang, J.; Duan, C. A Photoactive Basket-Like Metal–Organic Tetragon Worked as an Enzymatic Molecular Flask for Light Driven H₂ Production. *Chem. Commun.* **2013**, *49*, 627–629.

(57) He, C.; Lin, Z.; He, Z.; Duan, C.; Xu, C.; Wang, Z.; Yan, C. Metal-Tunable Nanocages as Artificial Chemosensors. *Angew. Chem., Int. Ed.* **2008**, *47*, 877–881.

(58) Huang, G.; Wang, S.; Ke, H.; Yang, L.; Jiang, W. Selective Recognition of Highly Hydrophilic Molecules in Water by Endo-Functionalized Molecular Tubes. *J. Am. Chem. Soc.* **2016**, *138*, 14550–14553.

(59) Zhao, L.; Jing, X.; Li, X.; Guo, X.; Zeng, L.; He, C.; Duan, C. Catalytic Properties of Chemical Transformation within the Confined Pockets of Werner-Type Capsules. *Coord. Chem. Rev.* **2019**, *378*, 151–187.

(60) Rittle, J.; Green, M. T. Cytochrome P450 Compound I: Capture, Characterization, and C–H Bond Activation Kinetics. *Science* **2010**, *330*, 933–937.

(61) Qian, Y.; Li, D.; Han, Y.; Jiang, H. Photocatalytic Molecular Oxygen Activation by Regulating Excitonic Effects in Covalent Organic Frameworks. *J. Am. Chem. Soc.* **2020**, *142*, 20763–20771.

(62) Wang, Y.; Li, J.; Liu, A. Oxygen Activation by Mononuclear Nonheme Iron Dioxygenases Involved in the Degradation of Aromatics. *J. Biol. Inorg. Chem.* **2017**, *22*, 395–405.

(63) Yuan, L.; Qi, M.-Y.; Tang, Z.-R.; Xu, Y.-J. Coupling Strategy for CO₂ Valorization Integrated with Organic Synthesis by Heterogeneous Photocatalysis. *Angew. Chem., Int. Ed.* **2021**, *60*, 21150–21172.

(64) Shi, W.; Quan, Y.; Lan, G.; Ni, K.; Song, Y.; Jiang, X.; Wang, C.; Lin, W. Bifunctional Metal–Organic Layers for Tandem Catalytic Transformations Using Molecular Oxygen and Carbon Dioxide. *J. Am. Chem. Soc.* **2021**, *143*, 16718–16724.

(65) Jing, X.; Yang, Y.; He, C.; Chang, Z.; Reek, J. N. H.; Duan, C. Control of Redox Events by Dye Encapsulation Applied to Light-Driven Splitting of Hydrogen Sulfide. *Angew. Chem., Int. Ed.* **2017**, *56*, 11759–11763.

(66) Knaus, T.; Paul, C. E.; Levy, C. W.; de Vries, S.; Mutti, F. G.; Hollmann, F.; Scrutton, N. S. Better than Nature: Nicotinamide Biomimetics That Outperform Natural Coenzymes. *J. Am. Chem. Soc.* **2016**, *138*, 1033–1039.

(67) Santi, N.; Morrill, L. C.; Świderek, K.; Moliner, V.; Luk, L. Y. P. Transfer Hydrogenations Catalyzed by Streptavidin-Hosted Secondary Amine Organocatalysts. *Chem. Commun.* **2021**, *57*, 1919–1922.

(68) Jeganathan, S.; Wendt, M.; Kiehstaller, S.; Brancaccio, D.; Kuepper, A.; Pospiech, N.; Carotenuto, A.; Novellino, E.; Hennig, S.; Grossmann, T. N. Constrained Peptides with Fine-Tuned Flexibility Inhibit NF- κ B Transcription Factor Assembly. *Angew. Chem., Int. Ed.* **2019**, *58*, 17351–17358.

(69) Manesis, A. C.; O’Connor, M. J.; Schneider, C. R.; Shafaat, H. S. Multielectron Chemistry within a Model Nickel Metalloprotein: Mechanistic Implications for Acetyl-CoA Synthase. *J. Am. Chem. Soc.* **2017**, *139*, 10328–10338.

(70) Mehta, R.; Rivera, D. D.; Reilly, D. J.; Tan, D.; Thomas, P. W.; Hinojosa, A.; Stewart, A. C.; Cheng, Z.; Thomas, C. A.; Crowder, M. W.; Alexandrova, A. N.; Fast, W.; Que, E. L. Visualizing the Dynamic Metalation State of New Delhi Metallo- β -Lactamase-1 in Bacteria Using a Reversible Fluorescent Probe. *J. Am. Chem. Soc.* **2021**, *143*, 8314–8323.

(71) Guengerich, F. P.; Child, S. A.; Barckhausen, I. R.; Goldfarb, M. H. Kinetic Evidence for an Induced-Fit Mechanism in the Binding of the Substrate Camphor by Cytochrome P450_{cam}. *ACS Catal.* **2021**, *11*, 639–649.

(72) Zhang, C.; Stone, E. A.; Deshmukh, M.; Ippolito, J. A.; Ghahremanpour, M. M.; Tirado-Rives, J.; Spasov, K. A.; Zhang, S.; Takeo, Y.; Kudalkar, S. N.; Liang, Z.; Isaacs, F.; Lindenbach, B.; Miller, S. J.; Anderson, K. S.; Jorgensen, W. L. Potent Noncovalent Inhibitors of the Main Protease of SARS-CoV-2 from Molecular Sculpting of the Drug Perampanel Guided by Free Energy Perturbation Calculations. *ACS Cent. Sci.* **2021**, *7*, 467–475.

(73) Groves, J. T.; Nemo, T. E.; Myers, R. S. Hydroxylation and Epoxidation Catalyzed by Iron-Porphine Complexes. Oxygen Transfer from Iodosylbenzene. *J. Am. Chem. Soc.* **1979**, *101*, 1032–1033.

(74) Green, D. W.; Sun, H.; Plapp, B. V. Inversion of the Substrate Specificity of Yeast Alcohol Dehydrogenase. *J. Biol. Chem.* **1993**, *268*, 7792–7798.

(75) Wodak, S. J.; Paci, E.; Dokholyan, N. V.; Berezovsky, I. N.; Horovitz, A.; Li, J.; Hilser, V. J.; Bahar, I.; Karanicolas, J.; Stock, G.; Hamm, P.; Stote, R. H.; Eberhardt, J.; Chebaro, Y.; Dejaegere, A.; Cecchini, M.; Changeux, J. P.; Bolhuis, P. G.; Vreede, J.; Faccioli, P.; Orioli, S.; Ravasio, R.; Yan, L.; Brito, C.; Wyart, M.; Gkeka, P.; Rivalta, I.; Palermo, G.; McCammon, J. A.; Panecka-Hofman, J.; Wade, R. C.; Di Pizio, A.; Niv, M. Y.; Nussinov, R.; Tsai, C. J.; Jang, H.; Padhorny, D.; Kozakov, D.; McLeish, T. Allostery in Its Many Disguises: From Theory to Applications. *Structure* **2019**, *27*, 566–578.